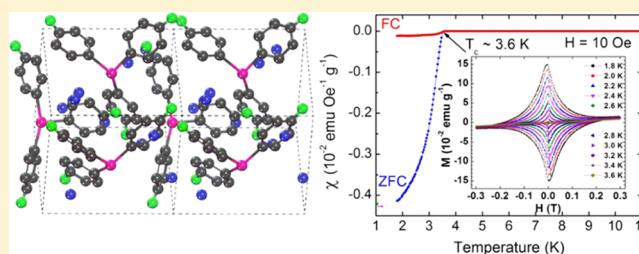


Discovery of Superconductivity in Potassium-Doped Tri-*p*-tolylbismuthine

HPSTAR
841-2019Ren-Shu Wang,^{†,‡,§} Hui Yang,^{†,§} Jia Cheng,[†] Xiao-Lin Wu,[†] Ming-An Fu,[†] Xiao-Jia Chen,^{*,†,‡,§} Yun Gao,^{*,†,‡,§} and Zhong-Bing Huang^{*,†,‡,§}[†]School of Materials Science & Engineering and Faculty of Physics & Electronic Technology, Hubei University, Wuhan 430062, China[‡]Center for High Pressure Science and Technology Advanced Research, Shanghai 201203, China

Supporting Information

ABSTRACT: Explorations of benzene-based organic superconductors and bismuth-based functional materials are today's hottest topics in chemistry, physics, and materials science. Here, we show that by doping potassium into an organobismuth molecule, tri-*p*-tolylbismuthine, which is composed of one bismuth atom and three methylphenyl groups, all synthesized samples exhibit type-II superconductivity at 3.6 K at ambient pressure and one sample also shows superconductivity at 5.3 K. The common 3.6 K superconducting phase is identified to have a triclinic P1 structure, with a mole ratio of 3:1 between potassium and tri-*p*-tolylbismuthine. The calculated electronic structure indicates that superconductivity is produced by transferring an electron from K 4s to the C 2p orbital, which results in both red and blue shifts of the Raman spectra. Our study enriches the physical functionality of organobismuth compounds and illustrates a new route for the search of organic superconductors.



INTRODUCTION

Organobismuth compounds have attracted growing interest over the past decades due to their unique properties and reactivity.^{1–3} As an environmentally friendly class of organic materials, different types of organobismuth compounds found applications in organic synthesis, catalysis, and functional materials. For instance, they have been widely used as reagents for arylation, cross-coupling, oxidation, and other reactions.^{4–8} Owing to the presence of a lone electron pair, trivalent organobismuthines can act as Lewis bases for catalytical reactions, such as carbon–carbon and carbon–heteroatom bond formations.⁹ In addition, organobismuth compounds have been used extensively as medicines for the treatment of gastrointestinal ailments, ulcers, tumor, and so forth.¹⁰

Despite remarkable progress made for organobismuth compounds, some reaction mechanisms need to be clarified and new properties are waiting to be discovered for enriching their functionalities. In particular, it is worth exploring superconducting (SC) property in benzene-based organobismuth compounds, arylbismuthines. On the one hand, superconductivity has been realized in various inorganic bismuth compounds, such as Bi₂Sr₂Ca_nCu_{n+1}O_{2n+6} (*n* = 0–2),^{11,12} BiTeCl,¹³ CoBi,¹⁴ Bi₄O₄S₃,¹⁵ RbBi_{11/3}Te₆,¹⁶ and topological insulators, such as Bi₂Se₃¹⁷ and Bi₂Te₃,¹⁸ among which bismuth copper oxides have SC transition temperatures up to 136 K at 36.4 GPa.¹² On the other hand, superconductivity was observed in various types of benzene-based systems, such as fullerides,^{19,20} graphites,^{21,22} graphene,^{23,24}

and aromatic hydrocarbons.^{25–31} A recent discovery of superconductivity at above 120 K in *p*-terphenyl^{32–34} and *p*-quaterphenyl³⁵ ignites the interest in high-temperature organic superconductors.^{36,37} In view of these facts, one interesting question arising is whether superconductivity and even high-temperature superconductivity exist in arylbismuthines.

Very recently, potassium-doped triphenylbismuth (TPB) was found to exhibit highly reproducible superconductivity at 3.5 and 7.2 K.³⁸ This finding opens a window for the search of organic superconductors in arylbismuthines. Here, we extend the exploration for superconductivity in potassium-doped tri-*p*-tolylbismuthine (*p*-TTB), in which three methyls are connected to TPB in the para position of the C–Bi bond. It is well known that the physicochemical properties of organic compounds can be tuned by various functional groups. For example, partial substitution of fluorine atoms with hydroxyl groups in fluorographene produces room-temperature organic magnets.³⁹ Methyl groups were found to reduce the energy gap of *N,N'*-diphenyl-dihydrodibenzo[*a,c*]phenazine and change its conformation from bent to a planar structure.⁴⁰ Therefore, potassium-doped *p*-TTB is expected to exhibit distinct physicochemical properties from the ones in potassium-doped TPB, which will be manifested by the SC transition temperatures, the mole ratio of potassium and the organo-

Received: March 26, 2019

Revised: June 17, 2019

Published: July 16, 2019

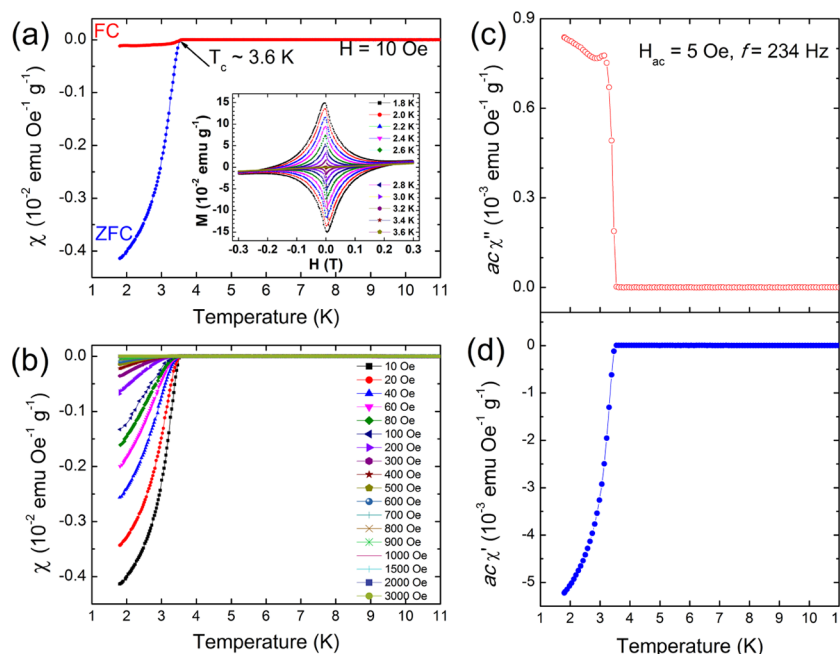


Figure 1. Temperature dependences of the dc and ac magnetic susceptibilities for sample pT1. (a) Temperature dependence of the dc magnetic susceptibility (χ) in the applied magnetic field of 10 Oe with field cooling (FC) and zero-field cooling (ZFC). The inset figure shows the magnetization loops at 1.8–3.6 K in the superconducting state. (b) Temperature dependence of the dc magnetic susceptibility (χ) measured at various magnetic fields in the ZFC run. (c, d) Imaginary (χ'') and real (χ') components of the ac magnetic susceptibility as a function of temperature. The probe harmonic magnetic field and frequency are 5 Oe and 234 Hz, respectively.

bismuth molecule, and the charge-transfer-induced Raman shifts.

METHODS

Material Synthesis. Potassium-doped *p*-TTB is synthesized by the two-step synthesis method, i.e., ultrasound treatment and low-temperature annealing.³⁸ High-purity potassium metal (99% purity, Sinopharm Chemical Reagent) was cut into small pieces and mixed with *p*-TTB (>98% purity, Tokyo Chemical Industry) with a mole ratio of *x*:1 (*x* = 2 and 3) in a glove box with the oxygen and moisture levels less than 0.1 ppm. Each mixture was then loaded into a quartz tube and sealed under high vacuum (1×10^{-4} Pa). The sample tubes were treated in an ultrasound device at 90 °C for 10 h to mix potassium and *p*-TTB thoroughly. After the ultrasound treatment, the sample tubes were heated at 130 °C for 3 days, followed by a slow cooling to room temperature.

Material Characterization. For each run of experiment, the sample from the same tube was distributed into several nonmagnetic capsules and sealed by GE varnish for following experimental measurements. Magnetization measurements were performed with a superconducting quantum interference device magnetometer (MPMS3, Quantum Design) in the temperature range of 1.8–300 K. The resistivity was measured in a physical property measurement system (PPMS, Quantum Design) with the help of a standard four-probe method. The crystal structure was measured on an X-ray diffraction (XRD) spectrometer (Bruker D8 advance). The Raman scattering spectra were collected at room temperature in an in-house system with a charge-coupled device and a spectrometer from Princeton Instruments in a wavelength of 660 nm and at a power less than 1 mW.

Computational Details. Our theoretical calculations were performed by a plane wave pseudopotential method as

implemented in the Vienna ab initio simulation package program.^{41,42} The generalized gradient approximation with the Perdew–Burke–Ernzerhof formula⁴³ for the exchange–correlation potentials and the projector-augmented wave method⁴⁴ for ionic potential were used to model the electron–electron and electron–ion interactions. Plane wave basis sets with an energy cutoff of 450 eV and a $3 \times 3 \times 3$ Monkhorst–Pack *k*-point mesh were adopted for geometry optimization. A finer $5 \times 5 \times 5$ *k*-point sampling scheme was used for calculating the partial density of states (PDOS). The convergence criteria for the energy and max force are set to 10^{-4} eV and 0.015 eV \AA^{-1} , respectively.

RESULTS AND DISCUSSION

Purchased *p*-TTB shows small positive magnetic susceptibility in the temperature range of 1.8–300 K (Supporting Information, Figure S1), different from the weak diamagnetic behavior for pristine *p*-TTB.⁴⁵ This difference can be ascribed to the paramagnetic impurities in purchased *p*-TTB. Upon doping potassium into *p*-TTB, superconductivity was first revealed by both the direct current (dc) and alternating current (ac) magnetization measurements in all synthesized samples. The representative results are summarized in Figure 1 for one sample with a mole ratio of 3:1 (labeled as pT1). Figure 1a shows the dc magnetic susceptibility (χ) for sample pT1 in the applied magnetic field of 10 Oe with field cooling (FC) and zero-field cooling (ZFC) in the temperature range of 1.8–11 K. Both FC and ZFC susceptibilities show a sudden decrease at around 3.6 K. Such a sudden drop of χ is originated from the well-defined Meissner effect, i.e., expulsion of magnetic field from a superconductor. The SC fraction at 1.8 K is estimated to be about 18%.

The inset of Figure 1a shows the magnetization loops of sample pT1 with the magnetic field up to 0.3 T measured in

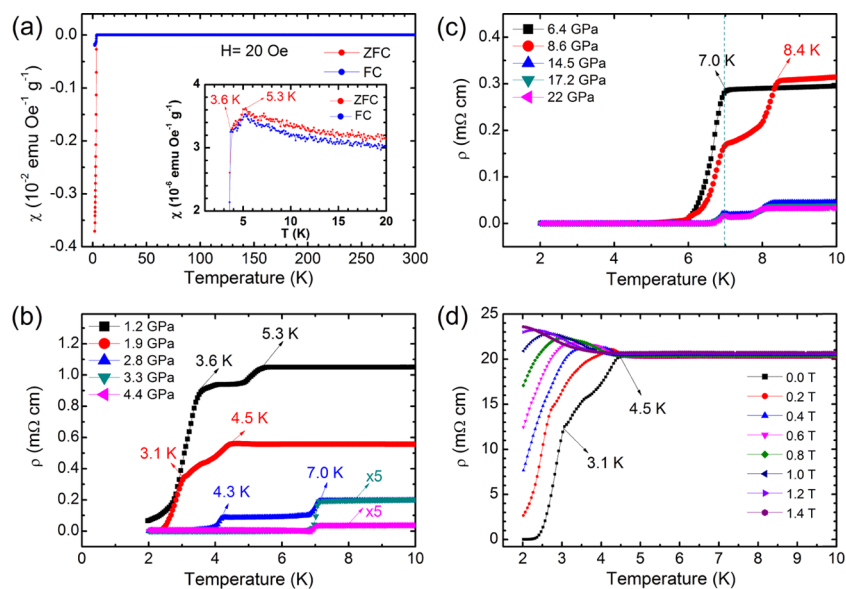


Figure 2. Temperature dependences of the dc magnetic susceptibility and resistivity for sample pT3. (a) Temperature dependence of the dc magnetic susceptibility (χ) in the applied magnetic field of 20 Oe with FC and ZFC. The inset figure shows the enlarged view of data below 20 K. (b, c) Temperature dependence of the resistivity under pressures of 1.2–4.4 and 6.4–22 GPa, respectively. (d) Temperature dependence of the resistivity measured at various magnetic fields under pressure of 1.9 GPa. The temperatures beside the arrows indicate the SC transition temperatures.

the temperature region 1.8–3.6 K. The hysteresis loops along the two opposite magnetic field directions show a clear diamond-like shape, providing strong evidence for the type-II superconductor. One can readily see that the dip or peak of the magnetization loop at 1.8 K appears at about 12 Oe magnetic field, indicating a very small lower critical magnetic field (H_{c1}) for the SC phase. The expansion of the diamond as the temperature decreases reflects the fact that the upper critical field (H_{c2}) increases with lowering the temperature. The obtained superconductivity in sample pT1 is also supported by the gradual shift of the χ - T curve toward a lower temperature with increasing the applied magnetic field, as shown in Figure 1b. This character is in accord with the intrinsic property of a superconductor, i.e., the SC transition temperature (T_c) is gradually reduced with the increase in magnetic field.

The ac magnetic susceptibility measurements were adopted to make a further confirmation for the observed superconductivity. The real component (χ') of the ac susceptibility is a measure of the magnetic shielding and the imaginary component (χ'') is related to energy dissipation in the sample due to the formation of SC vortex current.⁴⁶ Figure 1c,d presents the temperature dependence of χ'' and χ' of the ZFC ac susceptibility for sample pT1. As can be seen, both χ' and χ'' are close to zero above the SC transition due to the absence of flux exclusion in the normal state.

Upon entering the SC state below 3.6 K, the diamagnetic behavior leads to a negative χ' , which becomes more negative as more flux is expelled from the sample with lowering the temperature. It is interesting to notice that χ'' increases rapidly after the temperature is lowered to the onset point at 3.6 K and reaches a peak in a narrow temperature range of about 0.3–0.5 K. The χ'' peak is related to the situation when the ac field penetrates to the centers of sample grains.⁴⁶

The superconductivity at 3.6 K was also demonstrated in two samples with mole ratios of 2:1 (labeled as pT2, see Figure S2 in the Supporting Information) and 3:1 (labeled as pT3). The magnetic measurements for sample pT3 are shown in

Figure 2a. Besides the sudden drop of dc magnetic susceptibility (χ) at 3.6 K, the inset of Figure 2a shows that χ starts to decrease at around 5.3 K for both ZFC and FC runs. The SC fraction of sample pT3 estimated from the magnetic susceptibility at 1.8 K is 16%.

In Figure 2b,c, we show the temperature dependence of electrical resistivity (ρ) for sample pT3 at various pressures without applying the magnetic field. At 1.2 GPa, ρ exhibits an obvious downturn at around 5.3 K and a sharp drop at around 3.6 K. The position of downturn is in accordance with the temperature at which χ exhibits a weak anomaly, suggesting that there exists a new SC phase with T_c of about 5.3 K. The sharp drop of resistivity at around 3.6 K provides a complementary proof for the 3.6 K SC phase revealed by magnetic measurements. As the pressure is increased to 1.9 GPa, the positions of downturn and sharp drop shift to 4.5 and 3.1 K, respectively, indicating a suppression of superconductivity by pressure.

At a higher pressure of 2.8 GPa, two SC transitions appear at 4.3 and 7.0 K. The former can be reasonably attributed to the 4.5 K SC phase at 1.9 GPa, while the latter should originate from metal bismuth based on the following reasons. Notice that the 7.0 K SC phase persists in a wide pressure region from 2.8 to 22 GPa and meanwhile a SC phase at around 8.4 K appears above 8.6 GPa, as shown in Figure 2c. The starting pressures for the 7.0 and 8.4 K SC phases as well as their weak-pressure dependence are in good agreement with previous findings for compressed metal bismuth.⁴⁷ The existence of Bi in the synthesized samples is evidenced by the appearance of a colorless transparent liquid on the inner wall of the tube, indicating that partial *p*-TTB are decomposed into Bi atoms and methylphenyls. The obtained superconductivity in potassium-doped *p*-TTB is further confirmed by the temperature dependence of resistivity at a pressure of 1.9 GPa with applying magnetic fields up to 1.4 T, as displayed in Figure 2d. One can readily see that the resistivity curve systematically shifts toward lower temperatures with the increase in magnetic

field, signaling a suppression of superconductivity by magnetic field. When the magnetic field is increased from 0.0 to 0.2 T, the SC transition temperatures are reduced from 4.5 and 3.1 K to 4.2 and 2.7 K, respectively. Superconductivity is completely destroyed at 1.4 T in the studied temperature range. The evolution of resistivity and magnetic susceptibility (see Figures 1b and 2d) in the magnetic field, together with the Meissner effect and zero resistivity (see Figures 1a and 2b), unambiguously establishes superconductivity in potassium-doped *p*-TTB.

Due to the partial decomposition of *p*-TTB and closeness of 3.6 K to the T_c of KBi_2 (3.57 K),^{48–50} one may doubt that the 3.6 K SC phase observed in our samples probably corresponds to KBi_2 . This probability can be safely excluded based on the following reasons. First, the 3.6 K SC phase exhibits the type-II superconductivity with the upper critical field (H_{c2}) of up to 3000 Oe, while KBi_2 is a type-I superconductor with the critical field of about 160 Oe at 2.0 K.⁵⁰ In the ZFC run, an increase of magnetic field from 10 to 100 Oe reduces the SC transition temperature from 3.57 to 2.7 K for KBi_2 ⁵⁰ and from 3.6 to 3.45 K for sample pT1. Second, previous studies^{51–53} indicated that KBi_2 can only be formed in a Bi-rich environment (the mole fraction of Bi is larger than 0.65) and at temperatures above 260 °C, much higher than our annealing temperature. Therefore, it is hard to produce KBi_2 from potassium and decomposed *p*-TTB in our samples. To make a further exclusion of the contribution of K–Bi compounds to the SC phase, we annealed one sample with a mole ratio of 3:1 at 170 °C. It was found that a much more colorless liquid appears on the inner wall of the tube compared to the sample pT1 annealed at 130 °C, suggesting that more *p*-TTB molecules are decomposed with the increase in temperature. However, the SC fraction of the sample annealed at 170 °C is 4.3%, about one-fourth of the SC fraction for sample pT1. This result demonstrates that the 3.6 K SC phase is unlikely from KBi_2 or other K–Bi compounds, otherwise a higher SC fraction should be observed for the sample annealed at 170 °C since more K–Bi compounds could be formed from decomposed *p*-TTB.

X-ray diffraction (XRD) was employed to examine the evolution of the crystal structure from pristine to potassium-doped *p*-TTB. Figure 3 displays the XRD patterns of pristine *p*-TTB and sample pT3. Pristine *p*-TTB is a kind of molecular

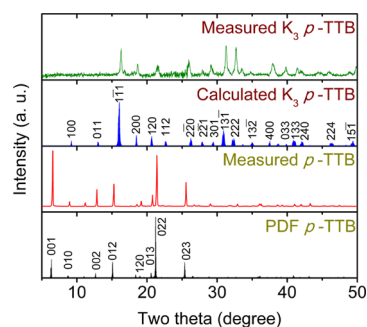


Figure 3. XRD patterns of pure and potassium-doped *p*-TTB. Measured K_3p -TTB and calculated K_3p -TTB represent the XRD patterns of sample pT3 and the theoretically predicted crystal structure, respectively. Measured *p*-TTB and PDF *p*-TTB correspond to the XRD patterns of the purchased and standard powder *p*-TTB, respectively. The experimental results were measured at room temperature, with the used X-ray wavelength being 1.54056 Å.

solid and crystallizes in the space group P1, as displayed in Figure 4a. The peak positions for the pristine material are in

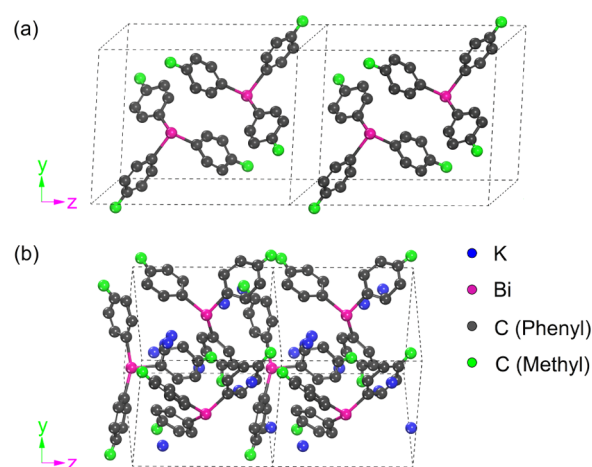


Figure 4. Structures and molecular arrangements of pure and potassium-doped *p*-TTB. (a) Molecular arrangement in pristine *p*-TTB is shown in a $2 \times 1 \times 1$ supercell. (b) Arrangement of molecules and potassium in the doped material is shown in a $2 \times 1 \times 1$ supercell. The black, green, purple, and blue balls represent carbon atoms in the phenyl rings, carbon atoms in the methyl groups, bismuth atoms, and potassium atoms, respectively. The hydrogen atoms are not shown in the figure for clarity.

good agreement with the ones in the standard PDF card. Upon potassium doping, no obvious peak appears at the positions where the pristine material shows strong peaks and the XRD feature is completely different from that of the undoped case. This indicates that the intercalation of potassium atoms into the interstitial space of methylphenyls and bismuth atoms produces a new crystal structure. The grain size derived from the Debye–Scherrer equation according to the first XRD peak of potassium-doped sample is 41 nm.

A comparison between the XRD patterns of potassium-doped TPB (see Figure 2 in ref 38) and *p*-TTB showed that the two systems have common main peaks at 16.1, 31.2, 32.5, and 37.8°, indicating that they crystallize into similar crystal structures. To identify the crystal structure of potassium-doped *p*-TTB, we replaced TPB with *p*-TTB in the unit cell of potassium-doped TPB and performed a full relaxation of atomic positions for the mole ratios of 3:1 and 4:1. The optimized results showed that the XRD pattern of 3:1 is in good agreement with the measured one, and the atomic positions of C, H, Bi, and K are given in the Supporting Information. In this crystal, three molecules of $\text{C}_{21}\text{H}_{21}\text{Bi}$ and nine K atoms distribute in a nearly cubic unit cell of dimensions $a = 9.57$ Å, $b = 9.61$ Å, $c = 9.58$ Å, $\alpha = 89.40^\circ$, $\beta = 90.29^\circ$, and $\gamma = 89.95^\circ$, as shown in Figure 4b. Potassium atoms represented by blue balls are intercalated in the interstitial space of bismuth and methylphenyl. Notice that the mole ratio for potassium-doped *p*-TTB is smaller than the one (4:1) for potassium-doped TPB. This can be ascribed to the steric hindrance of methyl groups that reduces the interstitial space for accommodating potassium atoms in the unit cell.

Figure 5a,b shows the band structures for pristine *p*-TTB and the doped material, and the corresponding partial density of states (PDOS) are presented in Figure 5c,d, respectively. It can be readily seen that pristine *p*-TTB is a semiconductor

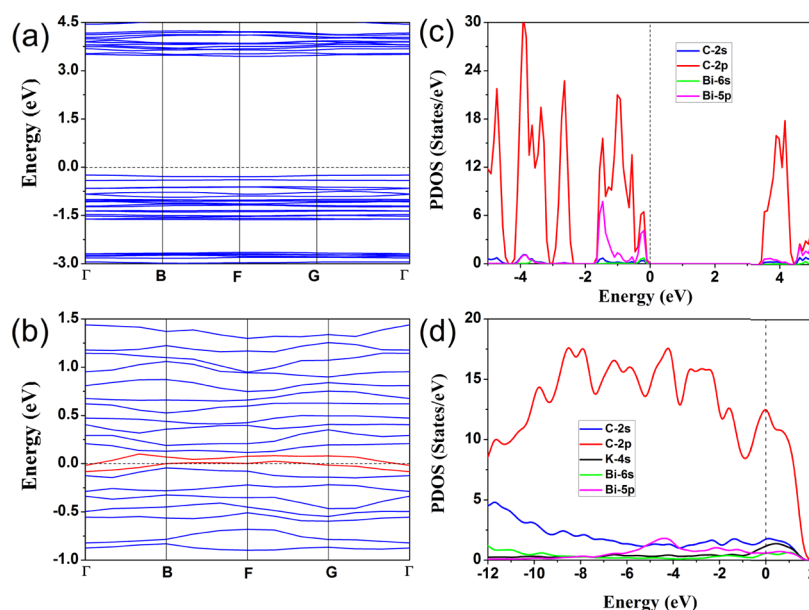


Figure 5. Energy band structures and orbital-resolved partial density of states (PDOS) of pure and potassium-doped *p*-TTB. (a, c) Energy band structure and PDOS of pristine *p*-TTB. (b, d) Energy band structure and PDOS of potassium-doped *p*-TTB. The Fermi energy is set to be zero. In (c) and (d), the red, blue, black, green, and purple solid lines represent PDOS of C 2p, C 2s, K 4s, Bi 6s, and Bi 5p orbitals, respectively.

with an energy gap of 3.39 eV near the Fermi level (dashed line). As can be seen from Figure 5b, the doped material becomes a metal, manifested by the Fermi level crossing two bands marked by red solid lines. Due to different arrangements of *p*-TTB molecules in the unit cell, the band structures are distinct for pristine and doped materials. Unlike the conventional n-type doping of semiconductors, where electrons transfer from dopants to the rigid conduction band, charge transfer and band reconstruction occur simultaneously in potassium-doped *p*-TTB. The PDOS in Figure 5c indicate that the energy states for pristine *p*-TTB are dominated by the C 2p orbital and the Bi 5p orbital also has an important contribution, while the C 2s and Bi 6s orbitals have a negligible contribution. For the doped case, the PDOS in Figure 5d indicates that the C 2p orbital makes a dominant contribution to the states in the vicinity of the Fermi level, while the K 4s orbital has a small contribution. This result not only reflects the fact that an electron is transferred from K 4s to the C 2p orbital but also demonstrates that the Fermi-level crossed bands, in Figure 5b, are formed by the lowest unoccupied molecular orbitals of phenyl rings.

The superconducting phase and charge transfer effect were further characterized by phase-sensitive Raman spectroscopy. Four regions of Raman-active modes from the low to high frequencies correspond to the lattice, C–C–C bending, C–H bending, and C–C stretching modes.^{54,55} We observed all of these modes in pristine *p*-TTB (Figure 6). Upon doping potassium into *p*-TTB, all lattice modes are dramatically suppressed.

Significant differences of the spectra between the pristine and doped samples are in the C–H bending and C–C stretching regions. Upon potassium doping, the C–H bending modes at 632, 1007, and 1048 cm⁻¹ in the pristine material shift down, while the pronounced modes at around 782 cm⁻¹ disappear in the Raman spectra. It is obvious that the mode intensity in the whole C–C stretching region gets a strong enhancement in the doped samples, which hints a strong polarization of phenyl rings. An upshift of Raman spectra of

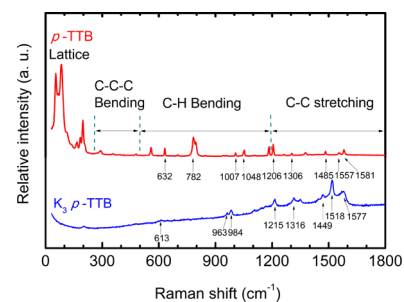


Figure 6. Raman scattering spectra of pristine and potassium-doped *p*-TTB collected at room temperature. Four regions of Raman-active modes, divided by the vertical dashed lines, are shown above the spectra of the pristine material. The inside numbers are the Raman shift values of different modes.

about 10 cm⁻¹ is observed for the two peaks at 1206 and 1306 cm⁻¹ in the pristine material, while the C–C stretching modes at 1485, 1557, and 1581 cm⁻¹ shift down by 36, 39, and 4 cm⁻¹, respectively. The observation of both red and blue shifts of Raman spectra in potassium-doped *p*-TTB is similar to the situation in potassium-doped TPB³⁸ but quite different from the situation in potassium-doped phenanthrene²⁶ and picene²⁸ wherein only red shifts were observed. As already pointed out in ref 38, the Raman shifts in our samples could be understood as the competing results between transferred electrons and enhanced polarization of phenyls, which is clearly manifested by the asymmetric Raman line shape and the increase of Raman intensity in the C–C stretching region. The former acts to soften the Raman modes, whereas the latter makes the Raman modes to shift up.⁵⁶ However, there exists an important difference in the Raman spectra of potassium-doped *p*-TTB and TPB; while the highest C–C stretching mode at 1581 cm⁻¹ in *p*-TTB shifts down slightly, the similar mode at 1564 cm⁻¹ in TPB shifts up by 20 cm⁻¹. This difference can be understood by taking the effect of the methyl group into account. Due to the similar electron-donating nature of the methyl group to Bi, its connection to the para position of the

C–Bi bond will reduce the polarization of phenyl rings. Therefore, the red shift of the highest C–C stretching mode in *p*-TTB can be attributed to the weakened polarization effect, which is overwhelmed by the charge-transfer-induced softening effect.

CONCLUSIONS

The present results provide unambiguous evidence for superconductivity at 3.6 and 5.3 K in potassium-doped *p*-TTB, which is suppressed by external pressures. The 3.6 K SC phase observed in all samples is identified to have a triclinic P1 structure with a mole ratio of 3:1 between potassium and *p*-TTB. Based on the theoretical calculations, it is shown that potassium-doped *p*-TTB lies in the metallic state with dominant C 2p states at the Fermi level and rearrangement of *p*-TTB molecules in the unit cell results in a distinct band structure from the semiconducting pristine material. The measured Raman spectra confirm the charge transfer from K 4s to the C 2p orbital and reveal the competing effect on the Raman shifts between transferred electrons and polarization of phenyls by Bi and methyl. Our findings are encouraging for the search of new organic superconductors in functional group-decorated triphenylbismuth.

ASSOCIATED CONTENT

Supporting Information

The Supporting Information is available free of charge on the ACS Publications website at DOI: 10.1021/acs.jpcc.9b02858.

Dc magnetic susceptibility for purchased *p*-TTB, dc and ac magnetic susceptibilities for sample pT2 with a mole ratio of 2:1 between potassium and *p*-TTB, and the CIF information for potassium-doped *p*-TTB (PDF)

AUTHOR INFORMATION

Corresponding Authors

*E-mail: xjchen@hpstar.ac.cn (X.-J.C.).

*E-mail: gaoyun@hubu.edu.cn (Y.G.).

*E-mail: huangzb@hubu.edu.cn (Z.-B.H.).

ORCID

Xiao-Jia Chen: 0000-0003-0673-8738

Yun Gao: 0000-0002-9898-5690

Zhong-Bing Huang: 0000-0003-2549-7917

Author Contributions

[§]R.-S.W. and H.Y. contributed equally to this work.

Notes

The authors declare no competing financial interest.

ACKNOWLEDGMENTS

This work was supported by the National Natural Science Foundation of China (Grants nos. 11574076, 11674087, and 91221103). The work at HPSTAR was supported by the National Key R&D Program of China (Grant no. 2018YFA0305900).

REFERENCES

- (1) Suzuki, H.; Matano, Y. *Organobismuth Chemistry*; Elsevier: Amsterdam, 2001.
- (2) Silvestru, C.; Breunig, H. J.; Althaus, H. Structural chemistry of bismuth compounds. I. organobismuth derivatives. *Chem. Rev.* **1999**, *99*, 3277–3328.

- (3) Breunig, H. J.; Rosler, R. New developments in the chemistry of organoantimony and -bismuth rings. *Chem. Soc. Rev.* **2000**, *29*, 403–410.

- (4) Ooi, T.; Goto, R.; Maruoka, K. Fluorotetraphenylbismuth: a new reagent for efficient regioselective α -phenylation of carbonyl compounds. *J. Am. Chem. Soc.* **2003**, *125*, 10494–10495.

- (5) Kayahara, E.; Yamago, S. Development of an arylthiobismuthine cocatalyst in organobismuthine-mediated living radical polymerization: applications for synthesis of ultrahigh molecular weight polystyrenes and polyacrylates. *J. Am. Chem. Soc.* **2009**, *131*, 2508–2513.

- (6) Luan, J. F.; Zhang, L. Y.; Hu, Z. T. Synthesis, properties characterization and applications of various organobismuth compounds. *Molecules* **2011**, *16*, 4191–4230.

- (7) Luqman, A.; Blair, V. L.; Bond, A. M.; Andrews, P. C. Formation of bismuth(V) thiolates: protolysis and oxidation of triphenylbismuth(III) with heterocyclic thiols. *Angew. Chem., Int. Ed.* **2013**, *52*, 7247–7251.

- (8) Worrell, B. T.; Ellery, S. P.; Fokin, V. V. Copper(I)-catalyzed cycloaddition of bismuth(III) acetylides with organic azides: synthesis of stable triazole anion equivalents. *Angew. Chem., Int. Ed.* **2013**, *52*, 13037–13041.

- (9) Gagnon, A.; Dansereau, J.; Le Roch, A. Organobismuth reagents: synthesis, properties and applications in organic synthesis. *Synthesis* **2017**, *49*, 1707–1745.

- (10) Keogan, D. M.; Griffith, D. M. Current and potential applications of bismuth-based drugs. *Molecules* **2014**, *19*, 15258–15297.

- (11) Maeda, H.; Tanaka, Y.; Fukutumi, M.; Asano, T. A new high-Tc oxide superconductor without a rare earth element. *Jpn. J. Appl. Phys.* **1988**, *27*, L209–L210.

- (12) Chen, X. J.; Struzhkin, V. V.; Yu, Y.; Goncharov, A. F.; Lin, C. T.; Mao, H. K.; Hemley, R. J. Enhancement of superconductivity by pressure-driven competition in electronic order. *Nature* **2010**, *466*, 950–953.

- (13) Ying, J. J.; Struzhkin, V. V.; Cao, Z. Y.; Goncharov, A. F.; Mao, H. K.; Chen, F.; Chen, X. H.; Gavriluk, A. G.; Chen, X. J. Realization of insulating state and superconductivity in the Rashba semiconductor BiTeCl. *Phys. Rev. B* **2016**, *93*, No. 100504(R).

- (14) Schwarz, U.; Tencé, S.; Janson, O.; Koz, C.; Krellner, C.; Burkhardt, U.; Rosner, H.; Steglich, F.; Grin, Y. CoBi₃: a binary cobalt-bismuth compound and superconductor. *Angew. Chem., Int. Ed.* **2013**, *52*, 9853–9857.

- (15) Singh, S. K.; Kumar, A.; Gahtori, B.; Shruti; Sharma, G.; Patnaik, S.; Awana, V. P. S. Bulk Superconductivity in bismuth oxysulfide Bi₄O₄S₃. *J. Am. Chem. Soc.* **2012**, *134*, 16504–16507.

- (16) Malliakas, C. D.; Chung, D. Y.; Claus, H.; Kanatzidis, M. G. Superconductivity in the narrow gap semiconductor RbBi_{11/3}Te₆. *J. Am. Chem. Soc.* **2016**, *138*, 14694–14698.

- (17) Kong, P. P.; Zhang, J. L.; Zhang, S. J.; Zhu, J.; Liu, Q. Q.; Yu, R. C.; Fang, Z.; Jin, C. Q.; Yang, W. G.; Yu, X. H.; et al. Superconductivity of the topological insulator Bi₂Se₃ at high pressure. *J. Phys.: Condens. Matter* **2013**, *25*, No. 362204.

- (18) Zhang, J. L.; Zhang, S. J.; Weng, H. M.; Zhang, W.; Yang, L. X.; Liu, Q. Q.; Feng, S. M.; Wang, X. C.; Yu, R. C.; Cao, L. Z.; et al. Pressure-induced superconductivity in topological parent compound Bi₂Te₃. *Proc. Natl. Acad. Sci. U.S.A.* **2011**, *108*, 24–28.

- (19) Hebard, A. F.; Rosseinsky, M. J.; Haddon, R. C.; Murphy, D. W.; Glarum, S. H.; Palstra, T. T. M.; Ramirez, A. P.; Kortan, A. R. Superconductivity at 18 K in potassium-doped C₆₀. *Nature* **1991**, *350*, 600–601.

- (20) Dahlke, P.; Denning, M. S.; Henry, P. F.; Rosseinsky, M. J. Superconductivity in expanded fcc C₆₀³⁻ fullerides. *J. Am. Chem. Soc.* **2000**, *122*, 12352–12361.

- (21) Emery, N.; Hérould, C.; d'Astuto, M.; Garcia, V.; Bellin, Ch.; Mareche, J. F.; Lagrange, P.; Loupiaz, G. Superconductivity of bulk CaC₆. *Phys. Rev. Lett.* **2005**, *95*, No. 087003.

- (22) Kim, J. S.; Boeri, L.; O'Brien, J. R.; Razavi, F. S.; Kremer, R. K. Superconductivity in heavy alkaline-earth intercalated graphites. *Phys. Rev. Lett.* **2007**, *99*, No. 027001.
- (23) Xue, M. Q.; Chen, G. F.; Yang, H. X.; Zhu, Y. H.; Wang, D. M.; He, J. B.; Cao, T. B. Superconductivity in potassium-doped few-layer graphene. *J. Am. Chem. Soc.* **2012**, *134*, 6536–6539.
- (24) Cao, Y.; Fatemi, V.; Fang, S.; Watanabe, K.; Taniguchi, T.; Kaxiras, E.; Jarillo-Herrero, P. Unconventional superconductivity in magic-angle graphene superlattices. *Nature* **2018**, *556*, 43–50.
- (25) Mitsuhashi, R.; Suzuki, Y.; Yamanari, Y.; Mitamura, H.; Kambe, T.; Ikeda, N.; Okamoto, H.; Fujiwara, A.; Yamaji, M.; Kawasaki, N.; et al. Superconductivity in alkali-metal-doped picene. *Nature* **2010**, *464*, 76–79.
- (26) Wang, X. F.; Liu, R. H.; Gui, Z.; Xie, Y. L.; Yan, Y. J.; Ying, J. J.; Luo, X. G.; Chen, X. H. Superconductivity at 5 K in alkali-metal-doped phenanthrene. *Nat. Commun.* **2011**, *2*, No. 507.
- (27) Xue, M. Q.; Cao, T. B.; Wang, D. M.; Wu, Y.; Yang, H. X.; Dong, X. L.; He, J. B.; Li, F. W.; Chen, G. F. Superconductivity above 30 K in alkali-metal-doped hydrocarbon. *Sci. Rep.* **2012**, *2*, No. 389.
- (28) Kambe, T.; He, X.; Takahashi, Y.; Yamanari, Y.; Teranishi, K.; Mitamura, H.; Shibusaki, S.; Tomita, K.; Eguchi, R.; Goto, H.; et al. Synthesis and physical properties of metal-doped picene solids. *Phys. Rev. B* **2012**, *86*, No. 214507.
- (29) Artioli, G. A.; Hammerath, F.; Mozzati, M. C.; Carretta, P.; Corana, F.; Mannucci, B.; Margadonna, S.; Malavasi, L. Superconductivity in Sm-doped [n]phenacenes (n = 3, 4, 5). *Chem. Commun.* **2015**, *51*, 1092–1095.
- (30) Gao, Y.; Wang, R. S.; Wu, X. L.; Cheng, J.; Deng, T. G.; Yan, X. W.; Huang, Z. B. Searching superconductivity in potassium-doped p-terphenyl. *Acta Phys. Sin.* **2016**, *65*, No. 077402.
- (31) Huang, G.; Zhong, G. H.; Wang, R. S.; Han, J. X.; Lin, H. Q.; Chen, X. J. Superconductivity and phase stability of potassium-doped p-quinquephenyl. *Carbon* **2019**, *143*, 837–843.
- (32) Wang, R. S.; Gao, Y.; Huang, Z. B.; Chen, X. J. Superconductivity above 120 kelvin in a chain link molecule, rXiv: 1703.06641. arXiv.org e-Print archive. <https://arxiv.org/abs/1703.06641> (submitted Mar 20, 2017).
- (33) Li, H.; Zhou, X.; Parham, S.; Nummy, T.; Griffith, J.; Gordon, K.; Chronister, E. L.; Dessau, D. S. Spectroscopic evidence of low energy gaps persisting towards 120 kelvin in surface-doped p-terphenyl crystals, arXiv: 1704.04230. arXiv.org e-Print archive. <https://arxiv.org/abs/1704.04230> (submitted Apr 13, 2017).
- (34) Liu, W. H.; Lin, H.; Kang, R. Z.; Zhu, X. Y.; Zhang, Y.; Zheng, S. X.; Wen, H. H. Magnetization of potassium-doped p-terphenyl and p-quaterphenyl by high-pressure synthesis. *Phys. Rev. B* **2017**, *96*, No. 224501.
- (35) Yan, J. F.; Zhong, G. H.; Wang, R. S.; Zhang, K.; Lin, H. Q.; Chen, X. J. Superconductivity and phase stability of potassium-intercalated p-quaterphenyl. *J. Phys. Chem. Lett.* **2019**, *10*, 40–47.
- (36) Zhong, G. H.; Wang, X. H.; Wang, R. S.; Han, J. X.; Zhang, C.; Chen, X. J.; Lin, H. Q. Structural and bonding characteristics of potassium-doped p-terphenyl superconductors. *J. Phys. Chem. C* **2018**, *122*, 3801–3808.
- (37) Carrera, M.; McDonald, J. L.; Untiedt, C.; Garcia-Hernandez, M.; Mompean, F.; Verges, J. A.; Guijarro, A. Characterization of main phase in K_p-terphenyl and its largest congener K_ppoly(p-phenylene): a report of their magnetic and electric properties. *J. Phys. Chem. C* **2019**, *123*, 5264–5272.
- (38) Wang, R. S.; Cheng, J.; Wu, X. L.; Yang, H.; Chen, X. J.; Gao, Y.; Huang, Z. B. Superconductivity at 3.5 K and/or 7.2 K in potassium-doped triphenylbismuth. *J. Chem. Phys.* **2018**, *149*, No. 144502.
- (39) Tucek, J.; Hola, K.; Bourlinos, A. B.; Blonski, P.; Bakandritsos, A.; Ugolotti, J.; Dubecky, M.; Karlicky, F.; Ranc, V.; Cepe, K.; et al. Room temperature organic magnets derived from sp³ functionalized graphene. *Nat. Commun.* **2017**, *8*, No. 14525.
- (40) Zhang, Z. Y.; Chen, C. L.; Chen, Y. A.; Wei, Y. C.; Su, J. H.; Tian, H.; Chou, P. T. Tuning the conformation and color of conjugated polyheterocyclic skeletons by installing ortho-methyl groups. *Angew. Chem., Int. Ed.* **2018**, *57*, 9880–9884.
- (41) Kresse, G.; Hafner, J. Ab initio molecular dynamics for liquid metals. *Phys. Rev. B* **1993**, *47*, No. 558(R).
- (42) Kresse, G.; Furthmüller, J. Efficient iterative schemes for ab initio total-energy calculations using a plane-wave basis set. *Phys. Rev. B* **1996**, *54*, 11169–11186.
- (43) Perdew, J. P.; Burke, K.; Ernzerhof, M. Generalized gradient approximation made simple. *Phys. Rev. Lett.* **1996**, *77*, 3865–3868.
- (44) Blöchl, P. E. Projector augmented-wave method. *Phys. Rev. B* **1994**, *50*, 17953–17979.
- (45) Gupta, R. R. *Landolt-Börnstein II/27 "Diamagnetic Susceptibility and Anisotropy"*; Springer, 2004.
- (46) Gömöry, F. Characterization of high-temperature superconductors by ac susceptibility measurements. *Supercond. Sci. Technol.* **1997**, *10*, 523–542.
- (47) Li, Y. F.; Wang, E. Y.; Zhu, X. Y.; Wen, H. H. Pressure-induced superconductivity in Bi single crystals. *Phys. Rev. B* **2017**, *95*, No. 024510.
- (48) Reynolds, J. M.; Lane, C. T. Superconducting bismuth alloys. *Phys. Rev.* **1950**, *79*, 405–406.
- (49) Ponou, S.; Müller, N.; Fässler, T. F.; Häussermann, U. KBi_{2-x}Pb_x (0 < x ≤ 1): a Zintl phase evolving from a distortion of the cubic Laves-phase structure. *Inorg. Chem.* **2005**, *44*, 7423–7430.
- (50) Sun, S. S.; Liu, K.; Lei, H. C. Type-I superconductivity in KBi₂ single crystal. *J. Phys.: Condens. Matter* **2016**, *28*, No. 085701.
- (51) Gnutzmann, G.; Klemm, W. The systems of potassium, rubidium and cesium with bismuth. *Z. Anorg. Allg. Chem.* **1961**, *309*, 181–188.
- (52) Petric, A.; Pelton, A. D. The Bi–K (bismuth–potassium) system. *J. Phase Equilib.* **1991**, *12*, 29–33.
- (53) Niu, C. J.; Li, C. R.; Du, Z. M.; Guo, C. P.; Liu, M. Thermodynamic assessment of the Bi–K binary system. *Thermochim. Acta* **2012**, *528*, 9–14.
- (54) Ludwig, C.; Götze, H. J. Fourier transform Raman and infrared spectra and normal coordinate analysis of (C₆H₅)₃Bi and (C₆D₅)₃Bi. *Spectrochim. Acta, Part A* **1995**, *51*, 2019–2026.
- (55) Shobatake, K.; Postmus, C.; Ferraro, J. R.; Nakamoto, K. Vibrational spectra of triphenyl compounds of group VA elements. *Appl. Spectrosc.* **1969**, *23*, 12–16.
- (56) Whiffen, D. H. Vibrational frequencies and thermodynamic properties of fluoro-, chloro-, bromo-, and iodo-benzene. *J. Chem. Soc.* **1956**, 1350–1356.